# Chapter 3
# AVO processing and AVO angle stacks results

## 3.1 AVO processing results

After all the processes; velocity analysis, normal moveout (NMO) correction, mute, parabolic Radon-transform demultiple, and stack were applied to both lines some remaining noises and multiples were removed. The final CDP gathers show the improved gathers after the Radon-transform demultiple was used and the full-fold stack sections show also clearer sections.

For this study, the AVO processing results in this section, are discussed and shown only the results of line B. The line A results are not discussed because they are similar to the results of line B.

Figure 3.1 shows the CDP gather 349 on line B before applied the Radon-transform demultiple but after NMO corrections and mute zoomed at 0.9 to 1.9 sec. In this study, all lithologic units between these two times are discussed. The CDP gather 349 is located right at Well C. Figure 3.2 shows the same CDP gather but after applied the Radon-transform demultiple. The red- and blue-box notations on the two figures show distinguished differences before and after applied the Radon-transform demultiple. It can be seen that the multiple at time about 1.0 sec was suppressed while the reflectors at time about 1.7 to 1.8 sec, which are the reflectors of gas sands, were continuous-improved reflectors. Although the Radon-transform demultiple results are not shown outstandingly differences on the CDP gathers, they can be effectively seen clearly differences on the stack sections.

Figure 3.3 shows the full-fold stack section of line B without the Radon-transform demultiple while the full-fold stack section of the same line but with the Radon-transform demultiple is shown in figure 3.4. The stack section after applied the Radon-transform demultiple show the clearer image which multiples were suppressed. The suppressions of multiples were clearly seen at time about 0.2 to 0.5 sec (blue box). However, not only multiples were eliminated at that range of times but they were suppressed at the times below the blue box as well. The main bright

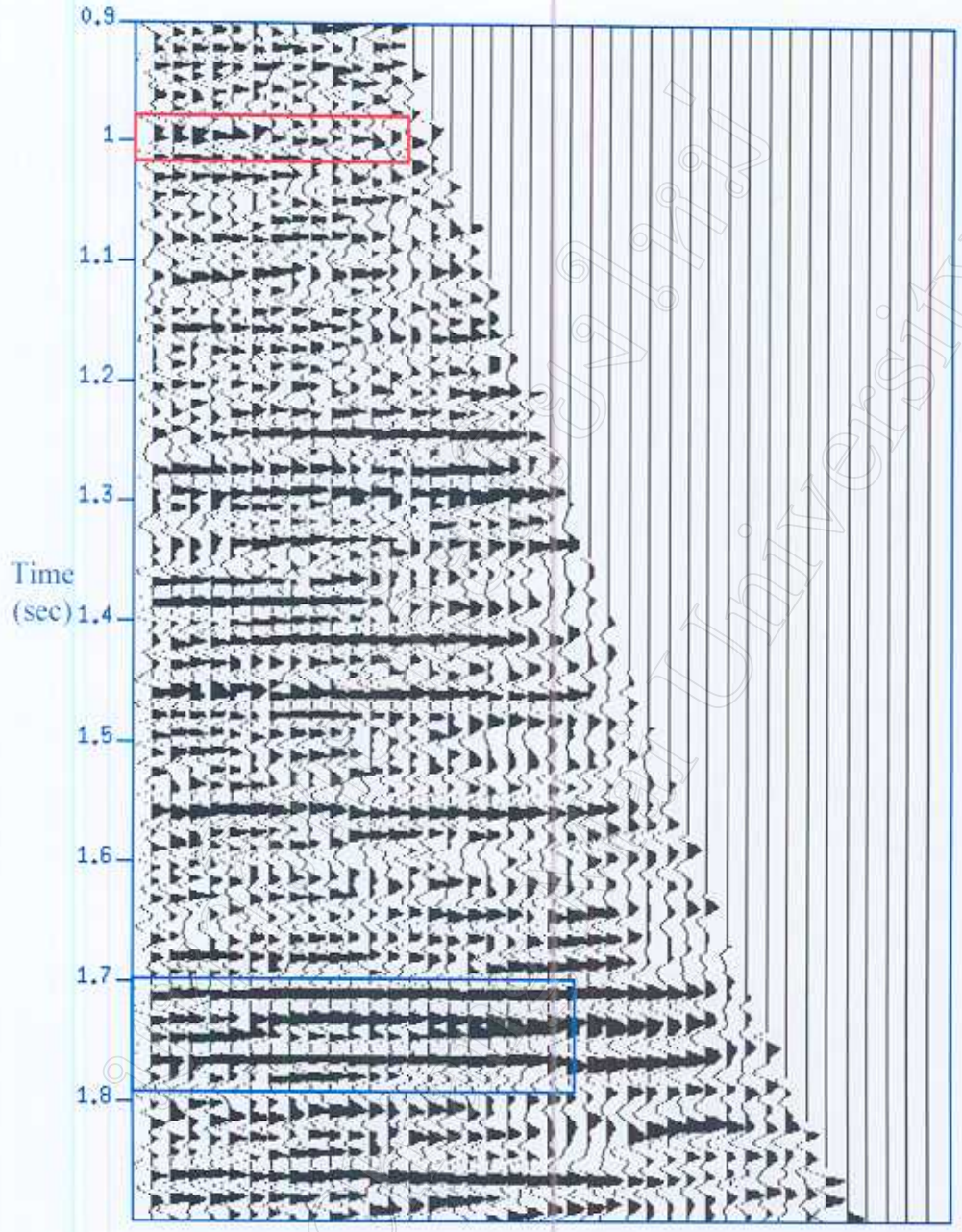


Figure 3.1 CDP gather 349 on line B before Radon demultiple but after NMO corrections and mute.

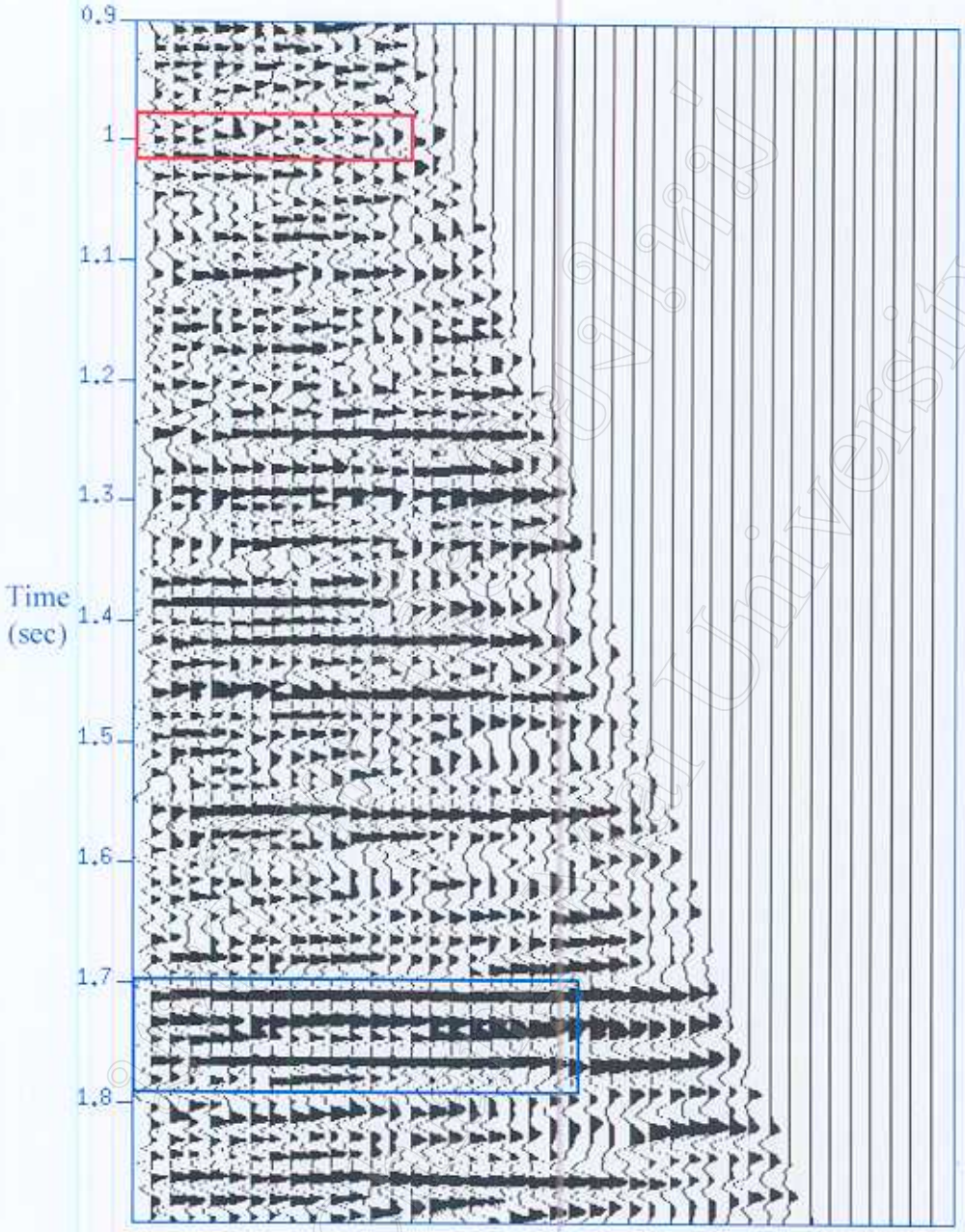


Figure 3.2 CDP gather 349 on Line B after Radon demultiple.

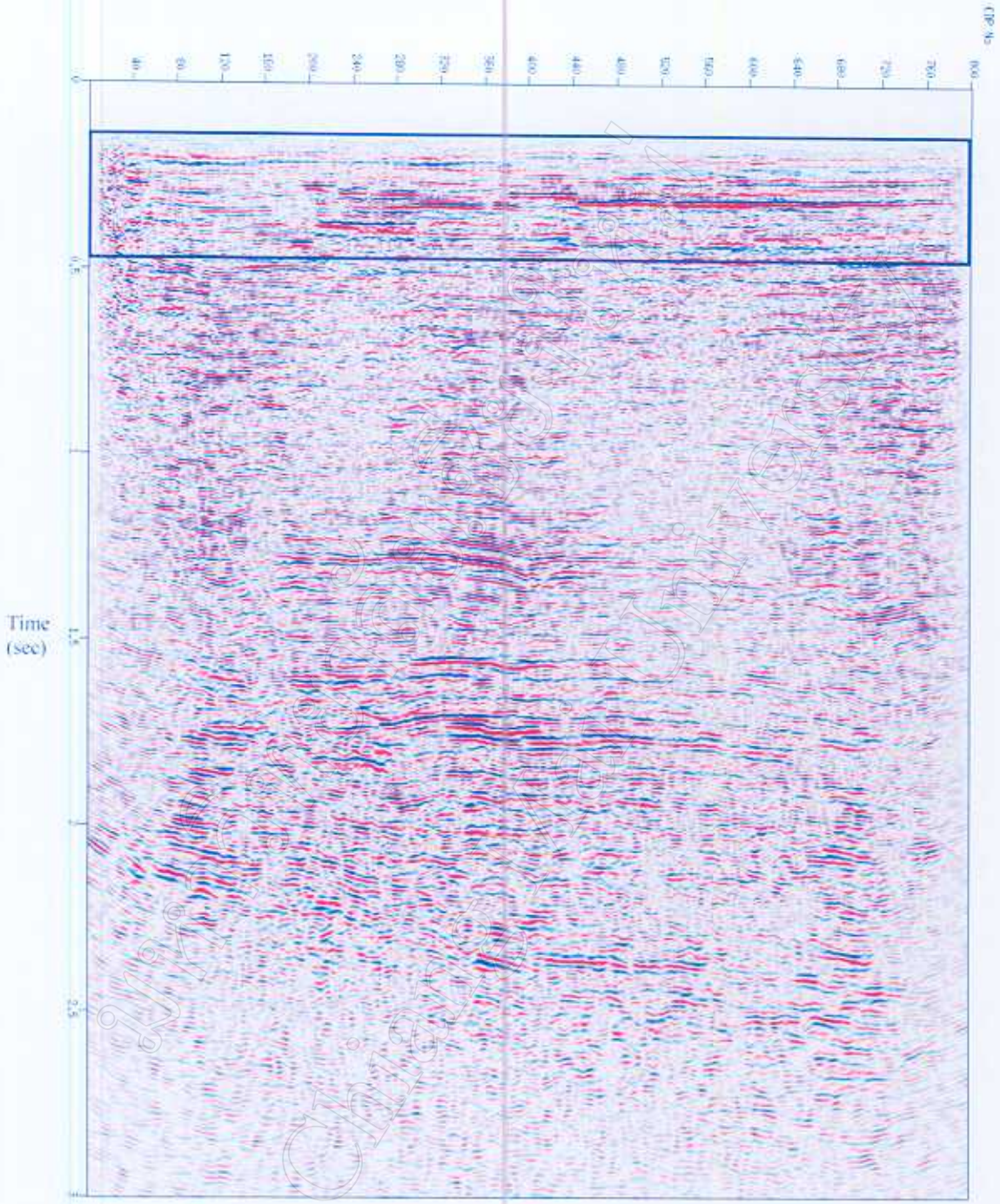


Figure 3.3 Full-fold stack section of line B without Radon demultiple.

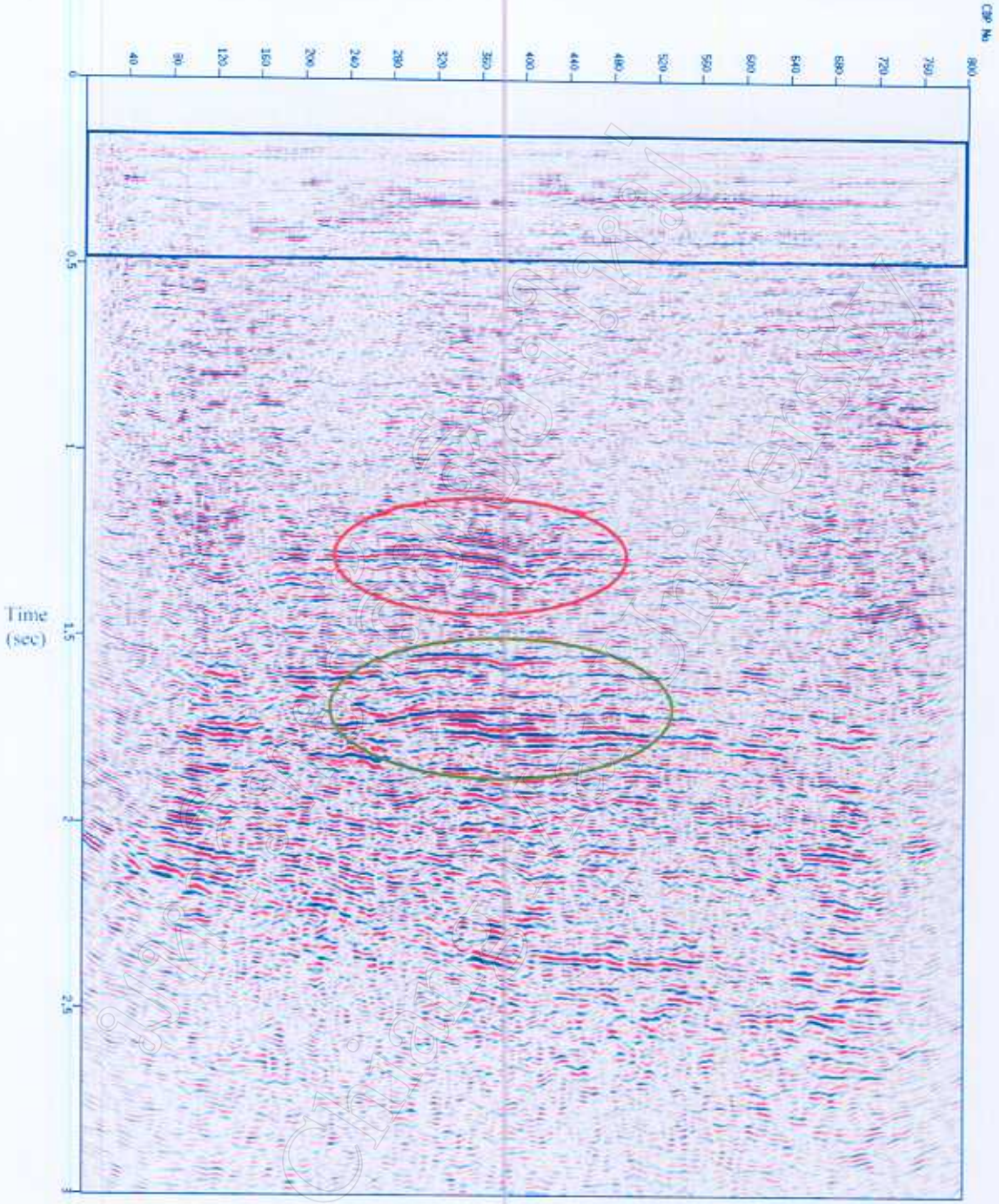


Figure 3.4 Full-fold stack section of line B with Radon demultiple.

spots on the stack section (red and green circles on figure 3.4) are shown more outstandingly after the remaining multiples were suppressed.

Figure 3.5 and 3.6 show respectively the full-fold stack section with and without the Radon-transform demultiple, which are zoomed at 0.9 to 1.9 sec. These figures do not show much different. However the figures show a bit more distinguished bright spot surrounding Well C location (CDP gather 349) and time around 1.7 to 1.8 sec, which is shown in the red circle. This bright spot is the gas sand anomaly that will be discussed in the next section, AVO angle stack results.

### 3.2 AVO angle stack results

The angle stacks of both lines gave the similar results thus only the results of line B are discussed in this section. The three angle-band stacks show the differences between each other. The amplitude of gas sands is stronger when angle band of stack increase.

Figure 3.7 shows the near-angle (0-15°) band of CDP gather 349 of line B zoomed at 0.9 to 1.9 sec. The figure shows an example of near-angle band pattern after the desired outside mute for near-angle band was applied to the Radon-transform demultiple CDP gathers. An example of middle-angle (15°-30°) band is shown in Figure 3.8, which is the CDP gather 349 of line B zoomed at 0.9 to 1.9 sec. The Figure 3.8 shows the result after the inside and the outside mutes for middle-angle band were applied to the Radon-transform demultiple CDP gathers of line B. Figure 3.9 shows the far-angle (30°-45°) band of CDP gather 349 of line B zoomed at 0.9 to 1.9 sec. The desired inside and outside mutes for far-angle band were applied and showed the results to the Radon-transform demultiple CDP gathers as an example gather in Figure 3.9.

After the three angle-band CDP gathers were obtained, they were stacked in order to achieve the three-propagation angle-band stack. The results of the angle-band stack are shown in Figure 3.10, Figure 3.11 and Figure 3.12.

Figure 3.10 shows the near-angle stack of line B. The middle-angle stack and the far-angle stack are shown in Figure 3.11 and Figure 3.12, respectively. All the three figures are zoomed at time 0.9 to 1.9 sec. The gas sand anomaly (in the red circle) is considered and discussed here.

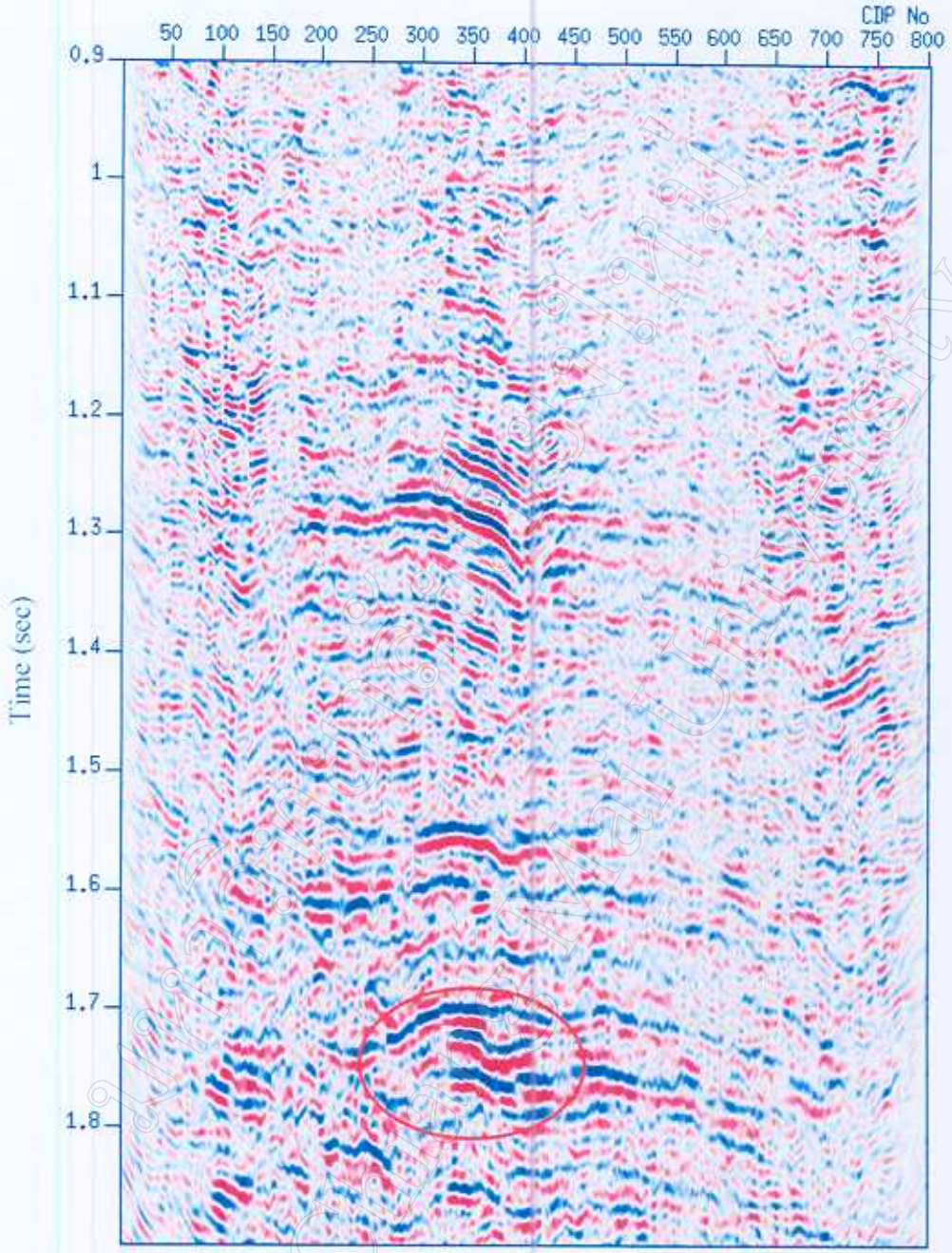


Figure 3.5 Full-fold stack section of line B without Radon demultiple, zoomed at 0.9-1.9 sec.

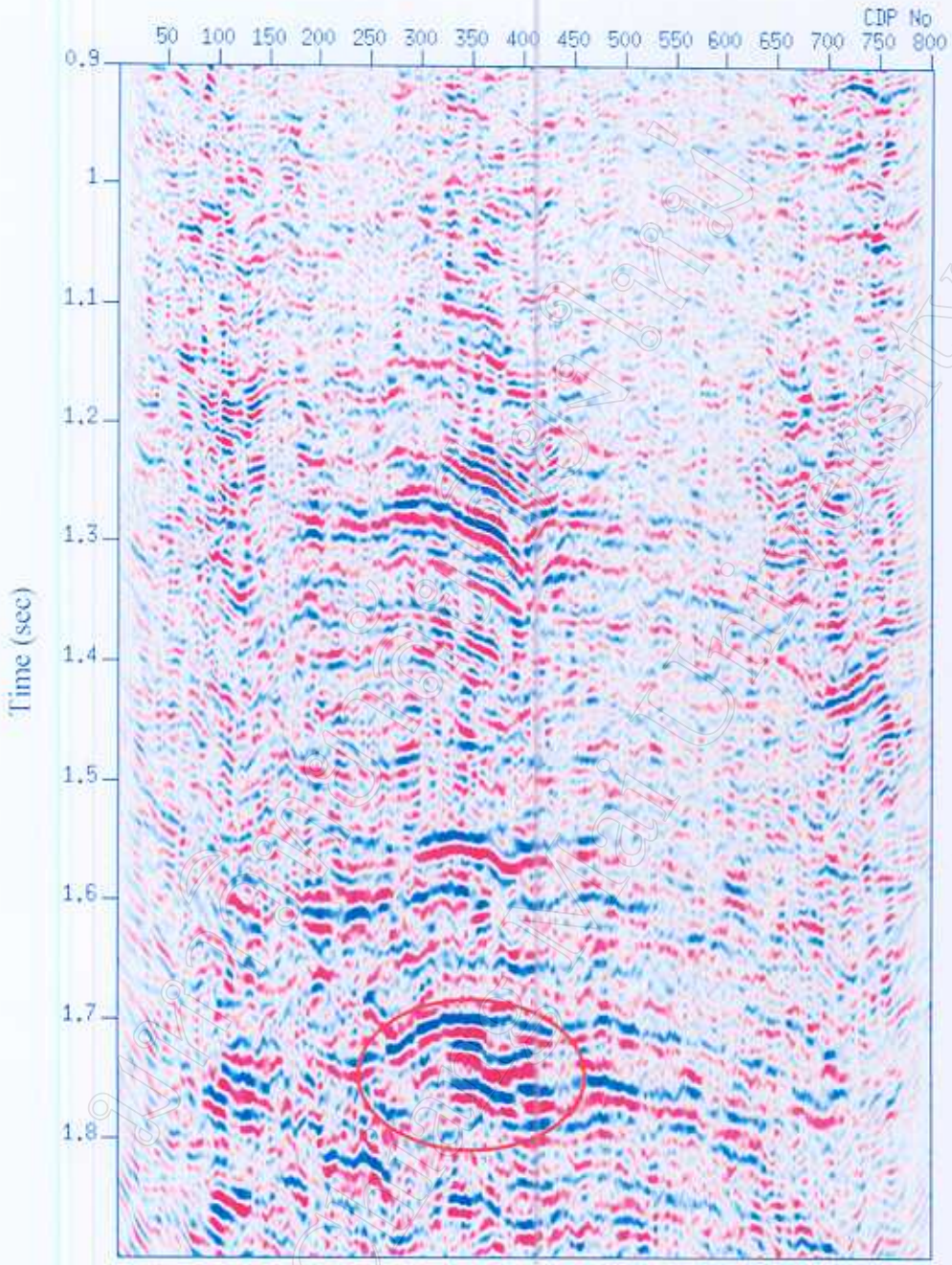


Figure 3.6 Full-fold stack section of line B with Radon demultiple, zoomed at 0.9-1.9 sec.

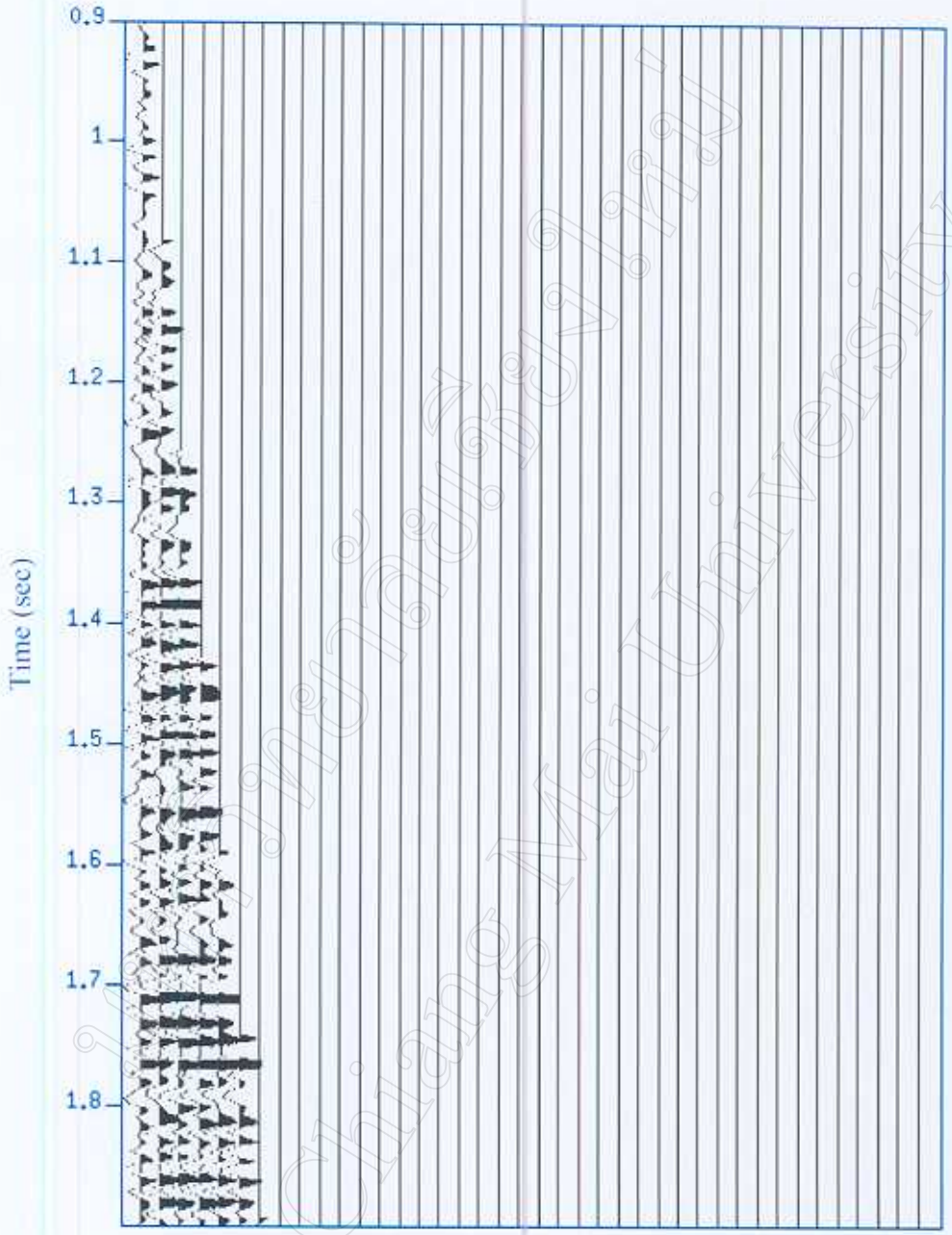


Figure 3.7 Near-angle (0° - 15°) band of CDP gather 349 of line B.

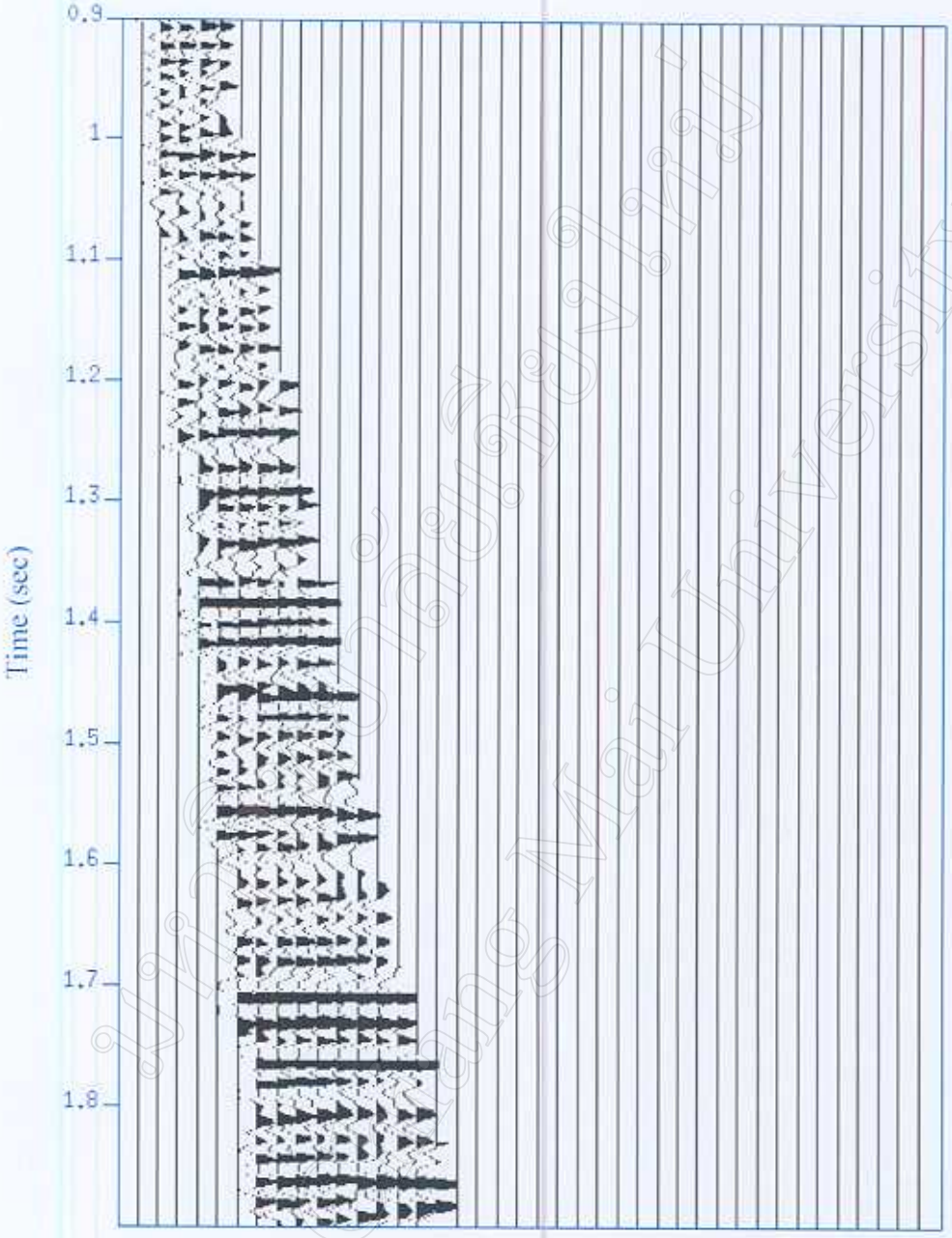


Figure 3.8 Middle-angle (15°- 30°) band of CDP gather 349 of line B.

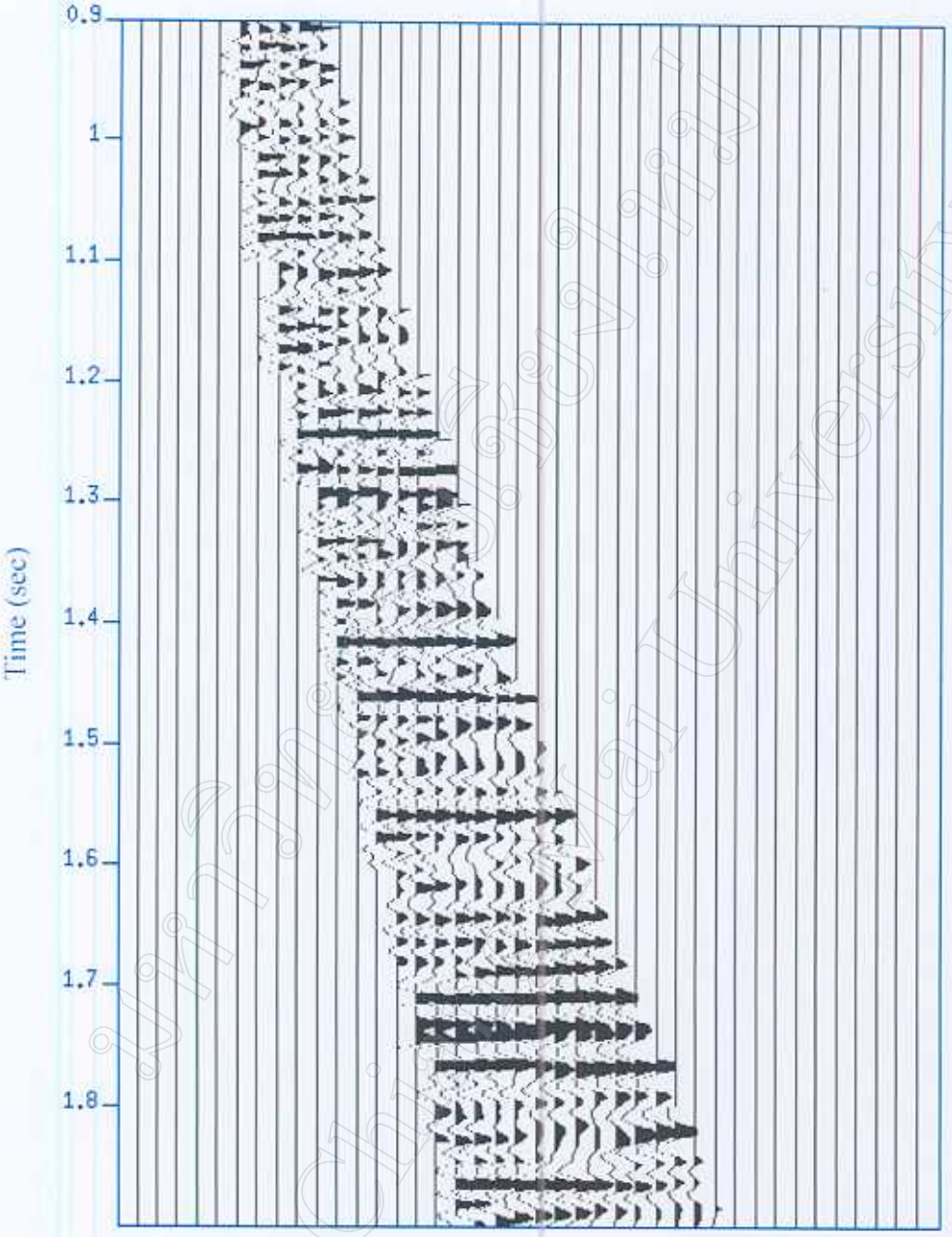


Figure 3.9 Far-angle (30° - 45°) band of CDP gather 349 of line B.

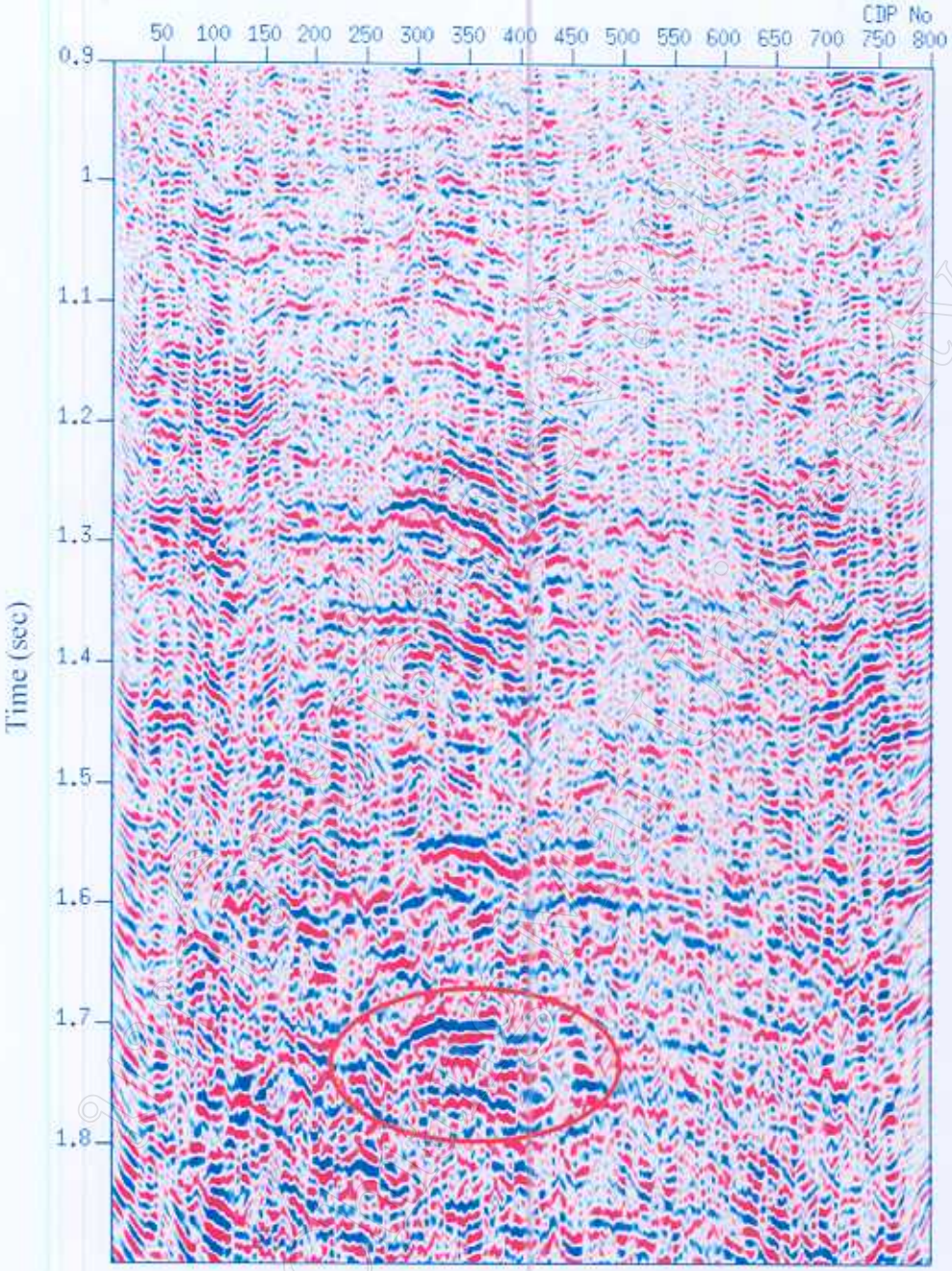


Figure 3.10 Near angle stack of line B.

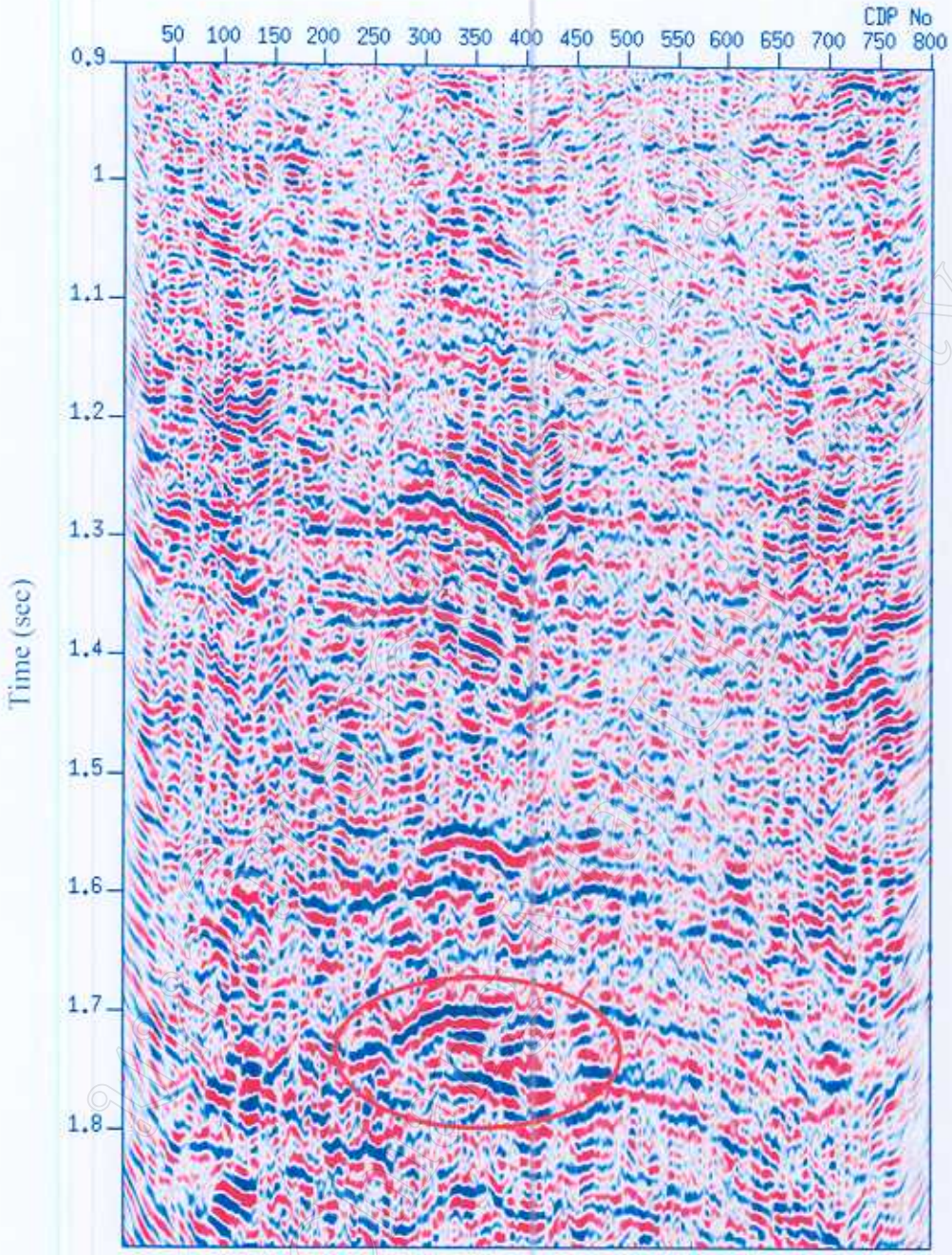


Figure 3.11 Middle-angle stack of line B.

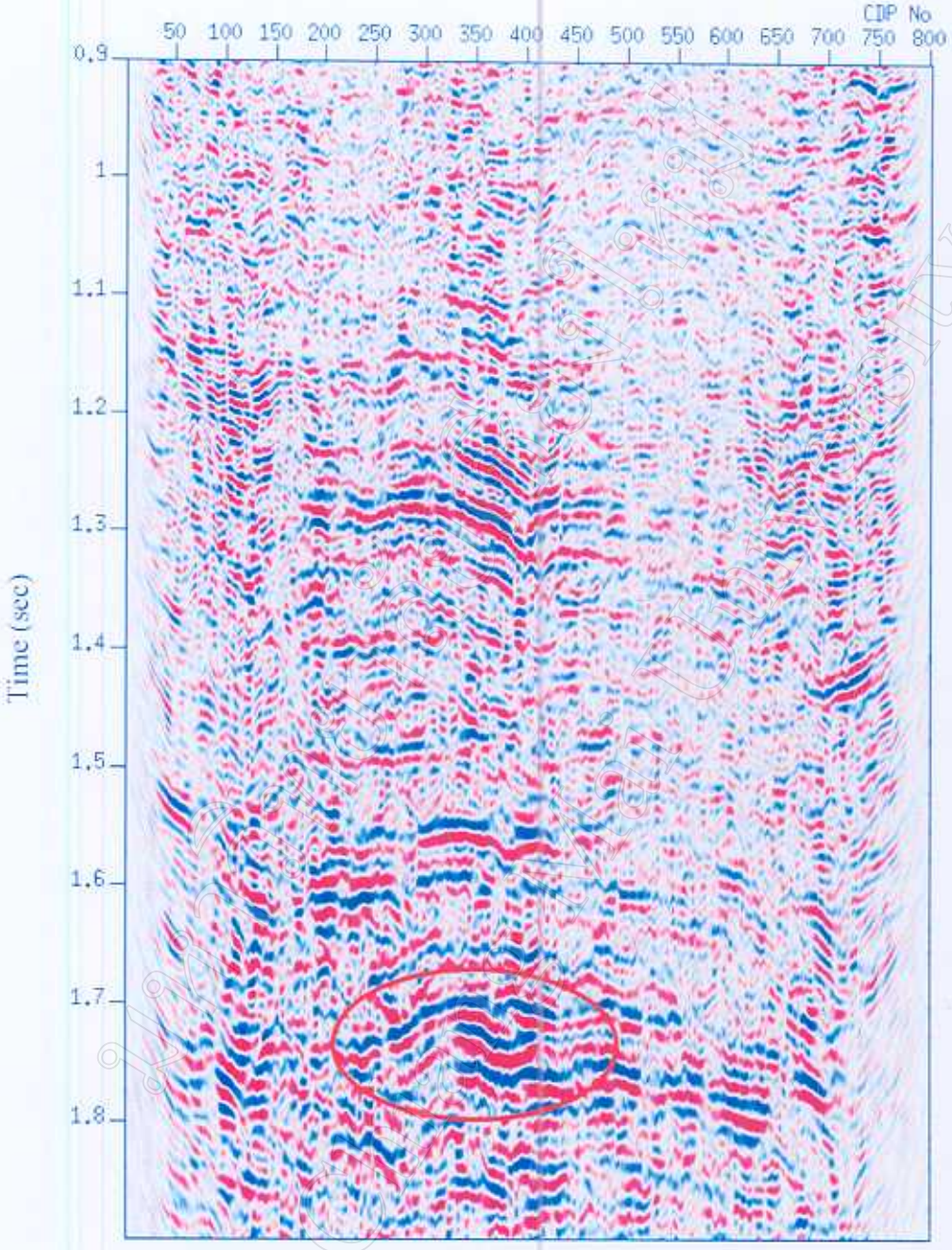


Figure 3.12 Far-angle stack of line B.

The gas sand shows the most prominent anomaly and strongest amplitude in the far-angle stack. The near-angle stack shows relatively unclear anomaly and weakest amplitude of gas sand. The gas sand anomaly on the middle-angle stack shows less prominent than the anomaly on the far-angle stack. The amplitude of gas sand on the middle-angle stack is also weaker than on the far-angle stack nevertheless it is stronger than the amplitude on the near-angle stack. Therefore it can be said that the gas sand amplitude anomaly show stronger and more prominently when the angle-band stack is higher.

The results of each angle-band stack subtraction are shown in Figure 3.13, Figure 3.14 and Figure 3.15. Figure 3.13 is the subtraction of near-angle stack from middle-angle stack of line B, Figure 3.14 is that of near-angle stack from far-angle stack, and Figure 3.15 is that of middle-angle stack from far-angle stack. The red circle notations in each figure are surrounded the area of gas sand amplitude. All the three figures show the sections with rather flat, not outstanding gas sand amplitude anomaly. However the anomaly on the three subtraction sections is more noticeable than any other anomaly in the sections. It can be seen that the gas sand amplitude of the subtraction of near-angle stack from far-angle stack is relatively strongest and most prominent. The gas sand amplitude of the subtraction of middle-angle stack from far-angle stack is less strong than that of the subtraction of near-angle stack from far-angle stack, but stronger than that of near-angle stack from middle-angle stack. From the entire angle stacks and their subtraction results, it can be inferred that the amplitude of gas sands in this study area have the trend that amplitude increases when propagation angle increases.

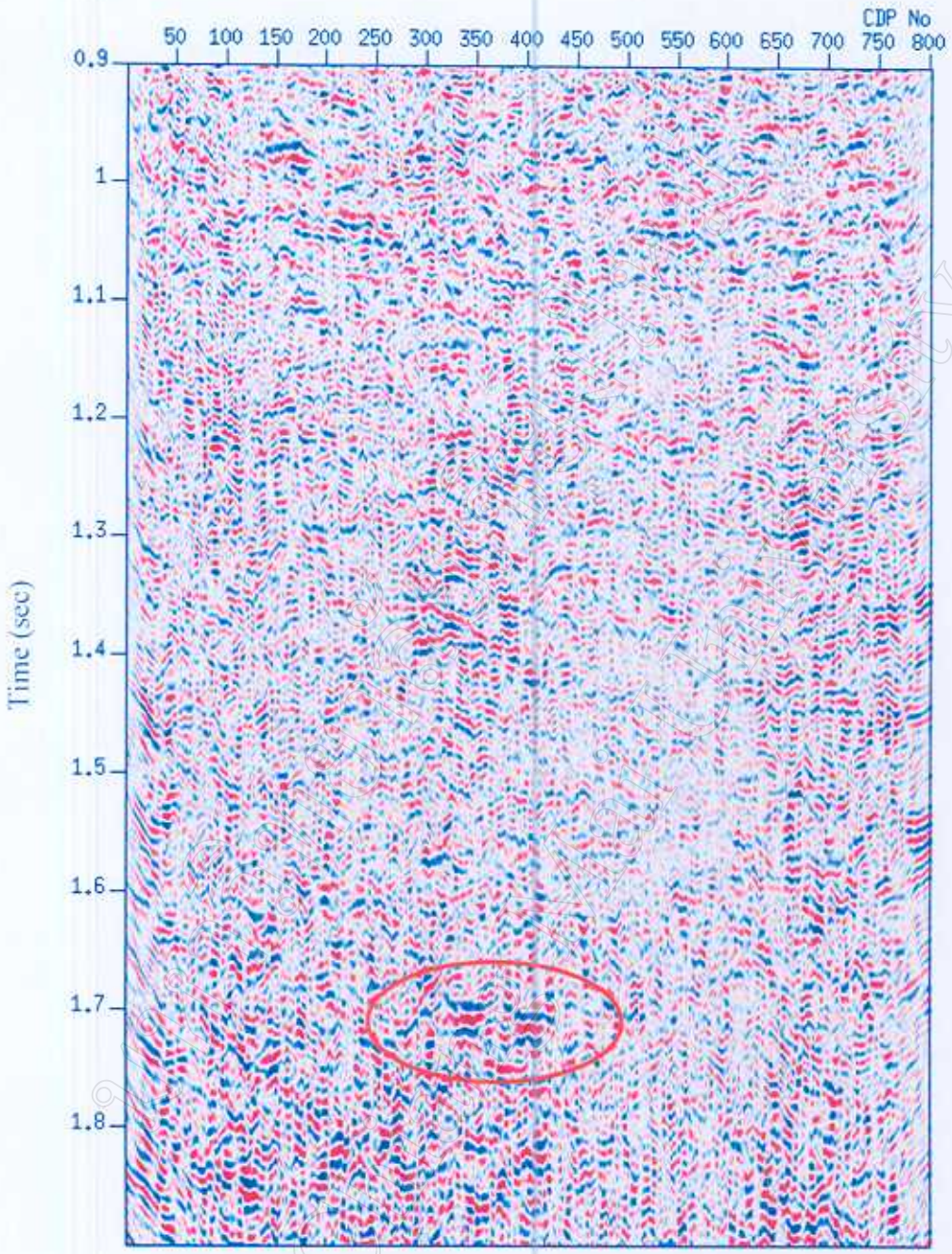


Figure 3.13 Subtraction of near-angle stack from middle-angle stack of Line B.

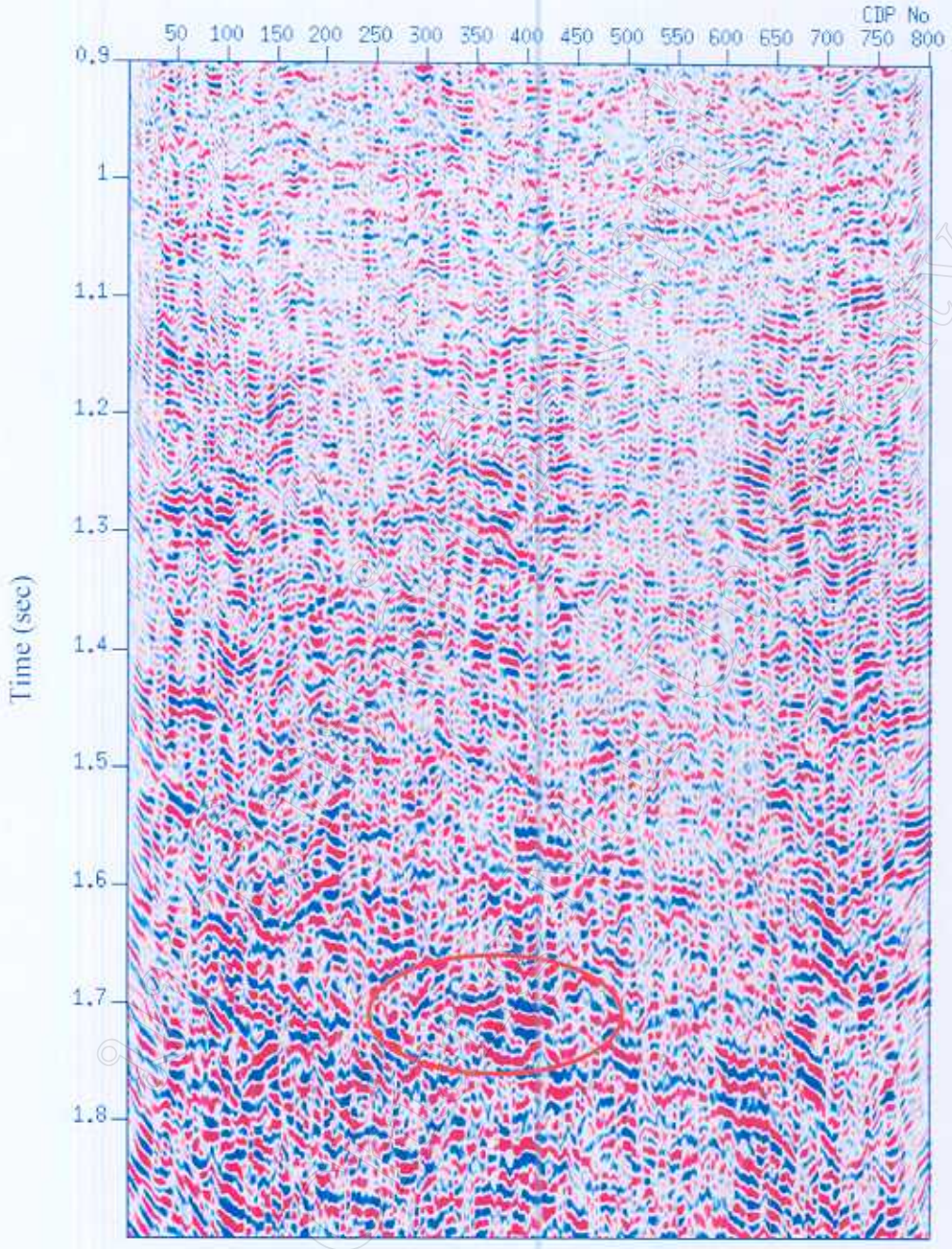


Figure 3.14 Subtraction of near-angle stack from far-angle stack of Line B.

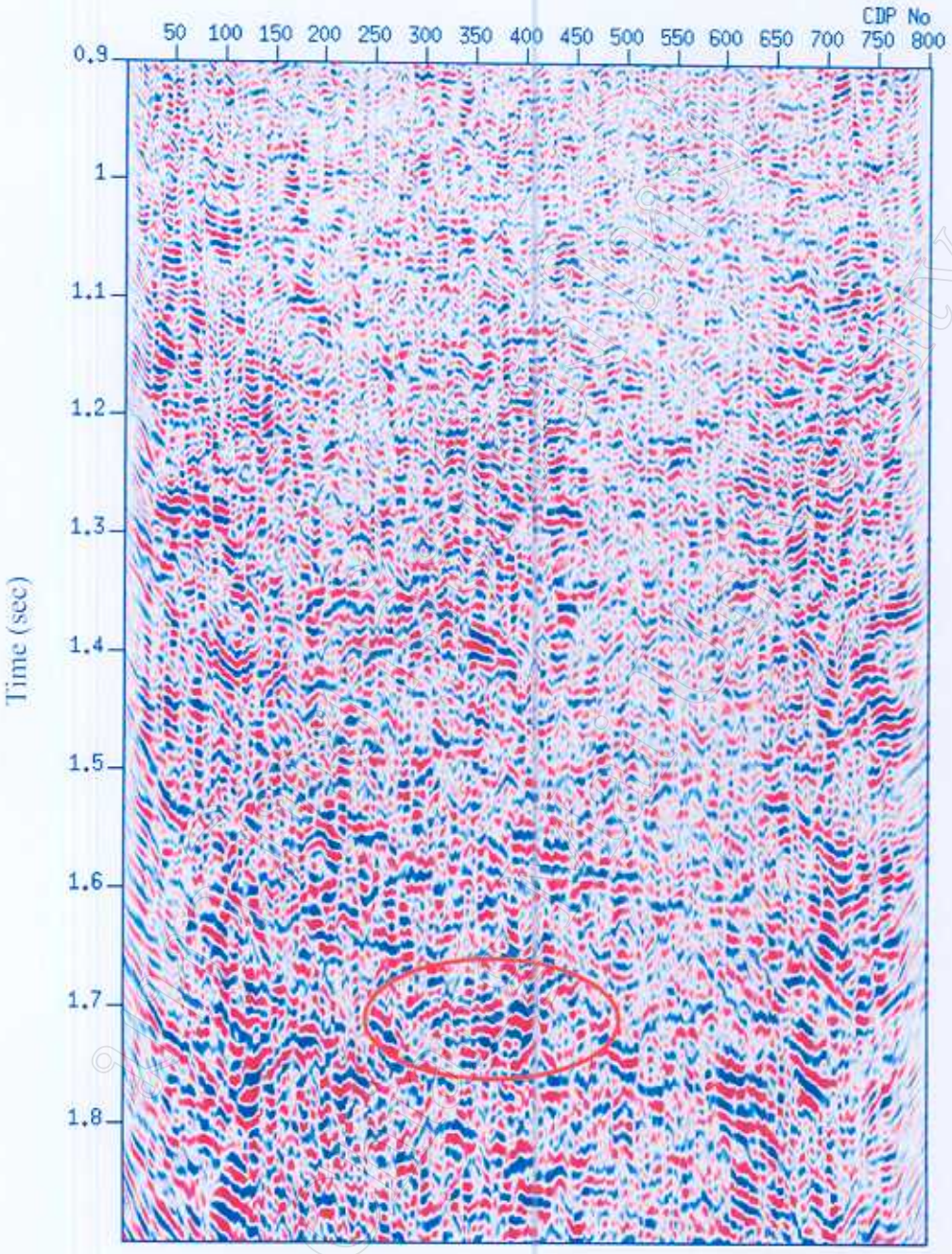


Figure 3.15 Subtraction of middle-angle stack from far-angle stack of Line B.